Neurobiology of Disease 198 (2024) 106558

Contents lists available at ScienceDirect

Neurobiology of Disease

journal homepage: www.elsevier.com/locate/ynbdi

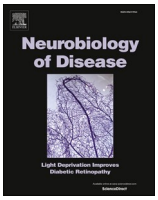

FLNA regulates neuronal maturation by modulating RAC1-Cofilin activity in the developing cortex

Antonio Falace [a,**,1], Lea Corbieres [b,1], Catia Palminha [b], Fabrizia Claudia Guarnieri [c,d], Fabienne Schaller [b], Emmanuelle Buhler [b], Clara Tuccari di San Carlo [e], Aurelie Montheil [b,f], Françoise Watrin [b], Jean Bernard Manent [b], Alfonso Represa [b], Antoine de Chevigny [b], Emilie Pallesi-Pocachard [b,f], Carlos Cardoso [b,*]

[a] *Pediatric Neurology and Muscular Diseases Unit, IRCCS Istituto "Giannina Gaslini", Genova, Italy*
[b] *INMED, INSERM UMR1249, Aix Marseille University, Parc Scientifique de Luminy, Marseille, France*
[c] *Institute of Neuroscience, National Research Council (CNR), Vedano al Lambro (MB), Italy*
[d] *IRCSS San Raffaele Scientific Institute, Milan, Italy*
[e] *Pediatric Neurology Unit and Laboratories, IRCCS Meyer Children's Hospital University of Florence, Firenze, Italy*
[f] *INMED, INSERM UMR1249, Aix Marseille University, Molecular and Cellular Biology Platform, Parc Scientifique de Luminy, Marseille, France*

ARTICLE INFO

Keywords:
Brain development
Neuronal maturation
Dendritogenesis -neurodevelopmental disorders
Animal model

SUMMARY

Periventricular nodular heterotopia (PNH), the most common brain malformation diagnosed in adulthood, is characterized by the presence of neuronal nodules along the ventricular walls. PNH is mainly associated with mutations in the *FLNA* gene – encoding an actin-binding protein - and patients often develop epilepsy. However, the molecular mechanisms underlying the neuronal failure still remain elusive. It has been hypothesized that dysfunctional cortical circuitry, rather than ectopic neurons, may explain the clinical manifestations. To address this issue, we depleted FLNA from cortical pyramidal neurons of a conditional $Flna^{flox/flox}$ mice by timed *in utero* electroporation of Cre recombinase. We found that FLNA regulates dendritogenesis and spinogenesis thus promoting an appropriate excitatory/inhibitory inputs balance. We demonstrated that FLNA modulates RAC1 and cofilin activity through its interaction with the Rho-GTPase Activating Protein 24 (ARHGAP24). Collectively, we disclose an uncharacterized role of FLNA and provide strong support for neural circuit dysfunction being a consequence of FLNA mutations.

Abbreviations: PNH, periventricular nodular heterotopia; FLNA, Filamin-A; RAC1, Rac Family Small GTPase 1; ARHGA24, Rho-GTPase Activating Protein 24; MCD, malformations of cortical development; Xq28, region q28 of the X Chromosome; flox, flanked by loxP; CAG, chicken beta-actin; CRE, Cre recombinase; LoxP, locus of crossover (x) P1; cKO, conditional knockout; CALNL, chicken actin loxP Neomycin loxP; GFP, Green fluorescent protein; IUE, *in utero* electroporation; E14.5, embryonic day 14.5; P6, postnatal day 6; NeuroD1, Neuronal Differentiation 1; ND1, NeuroD1; P15, postnatal day 15; DsRed, red fluorescent protein; FingR, recombinant fibronectin intrabodies generated by mRNA display; PSD, postsynaptic density; GTP, Guanosine-5′-triphosphate; ADF, actin depolymerizing factor; S3A, Serine3Alanine; T17N, Threonine17Asparagine; Q61L, Glutamine61Leucine; GAP, GTPase-activating protein; TSC, Tuberous Sclerosis Complex 1; MEK, Mitogen-activated protein kinase kinase; ERK, extracellular signal-regulated kinase; Rheb, Ras homolog enriched in brain; mTORC1, mammalian target of rapamycin complex 1; rpS6, ribosomal protein S6; mTOR, mechanistic target of rapamycin; PAC, P21 Activated Kinase 1; LIMK, LIM Domain Kinase 1; F-actin, filamentous actin; FMR1, Fragile X Messenger Ribonucleoprotein 1; Shank3B, SH3 And Multiple Ankyrin Repeat Domains 3B; FCD, focal cortical dysplasia; PTI-25, 1-benzyl-8-methyl-1,4,8-triazaspiro[4.5]decan-2-one (Simufilam); SEM, Standard error of the mean; Tbr1, T-Box Brain Transcription Factor 1; CDP, centromere binding factor; GST, Glutathione transferase; SDS-PAGE, Sodium dodecyl-sulfate polyacrylamide gel electrophoresis; PBD, p21-binding domain; RIPA, radioimmunoprecipitation assay buffer; BCA, Bicinchoninic acid assay; ANOVA, analysis of variance..

* Corresponding author at: INMED, INSERM UMR1249, Parc Scientifique de Luminy, BP13, 13009 Marseille, France.
** Corresponding author at: IRCCS Istituto "Giannina Gaslini", Pediatric Neurology and Muscular Diseases Unit, Largo Gaslini 5, 16147 Genova, Italy.
E-mail addresses: antoniofalace@gaslini.org (A. Falace), carlos.cardoso@inserm.fr (C. Cardoso).
[1] Equally contributing authors.

https://doi.org/10.1016/j.nbd.2024.106558
Received 12 July 2023; Received in revised form 5 June 2024; Accepted 5 June 2024
Available online 7 June 2024

1. Introduction

The cerebral cortex plays key roles in learning, memory, sensory and motor functions (Kandel and Squire, 2000). The proper execution of these tasks depends on stereotypically organized and functional neural networks. Neural circuit connectivity is the endpoint of a long process of embryonic and postnatal cortical development, which relies on the generation and specification of a multitude of neuronal subtypes, their migration to appropriate layers and the establishment of synaptic connections between them (Ayala et al., 2007; Rakic, 2009; Kaas, 2013; Lodato and Arlotta, 2015). Alterations in any of these processes, due to genetic mutations or environmental insults (*e.g.* vascular injury, viral infection *in utero*), lead to malformations of cortical development (MCD). Although each individual MCD phenotype is considered rare, altogether MCDs represent a major cause of drug-resistant epilepsy, autism and intellectual disability (Guerrini and Dobyns, 2014; Guarnieri et al., 2018).

The most frequent form of MCD, Periventricular Nodular Heterotopia (PNH), is characterized by the presence of ectopic neuronal nodules lining the lateral ventricles. The majority of affected patients often have seizures and display average cognitive abilities despite the striking changes in grey matter architecture (Aghakhani et al., 2005; Parrini et al., 2006). Seizures occur most often in childhood, but the age of seizure onset varies from the neonatal period to adulthood (Parrini et al., 2006). The severity of seizures may range from mild, with rare episodes and spontaneous remission without need of antiepileptic drugs, to untreatable (Dubeau et al., 1995). Mutations in the *Filamin A* (or *FLNA*) gene on Xq28 are the main cause of PNH (Parrini et al., 2006; Fox et al., 1998). *FLNA* encodes a large (280 kDa) cytoplasmic dimeric actin-binding phospho-protein, which promotes cross-linking of F-actin filaments into orthogonal networks, thus tuning the elastic properties of the cytoskeleton (Gardel et al., 2006; Sutherland-Smith, 2011). The FLNA protein integrates extracellular signaling and cell adhesion with cytoskeletal organization, and mediates cell reshaping and migration predominantly through actin effectors such as the Rho-GTPases (Sutherland-Smith, 2011; Nakamura et al., 2009; Sheen, 2014). The expression of FLNA is widespread in developing cortex, particularly in radial glial cells, and persists in the adult brain in neuroependymal cells and in pyramidal neurons throughout layers II to VI (Sheen et al., 2002; Carabalona et al., 2012; Lian et al., 2012; Noam et al., 2012). In excitatory neurons, FLNA has been detected in the somato-dendritic compartment, including in dendritic spines (Noam et al., 2012; Segura et al., 2016). In rodents, complete *Flna* depletion results in embryonic lethality due to severe cardiovascular defects (Feng et al., 2006; Hart et al., 2006). In contrast, *in utero* knockdown of *Flna* in neural progenitors, leads to the formation of PNH lining the ventricular surface that results from disruption of both the polarized radial glial scaffold and the neuroepithelial lining (Carabalona et al., 2012). Interestingly, a similar phenotype was observed in brain biopsies from PNH patients carrying *a FLNA* mutation, which display clear discontinuity in the neuroepithelial lining (Carabalona et al., 2012; Ferland et al., 2009).

Although the link between PNH and clinical manifestations has been well established, the functional relationships between ectopic neurons and cortical structures remain uncertain. Indeed, no correlation between the extent of PNH and epilepsy severity was found (Parrini et al., 2006; Solé et al., 2009), and only a very little percentage of interictal epileptiform discharges are purely heterotopic in patients (6% of the cases) (Pizzo et al., 2017). Moreover, *FLNA* mutations in epileptic patients without PNH visible by brain imaging were reported (Wei et al., 2018; Hiromoto et al., 2020). These data support the hypothesis that cortical circuit dysfunction, rather than ectopic neurons, may explain the occurrence of seizures and cognitive impairment (Staley, 2015; Lee et al., 2017; Bozzi et al., 2018). However, the intrinsic role of FLNA in neural circuit formation and function still remains undetermined.

To address this issue, we deleted *Flna* from a fraction of layer II-III pyramidal neurons by timed *in utero* electroporation of Cre recombinase into developing *Flna*$^{flox/flox}$ mouse ventricular zone. Sparse depletion of *Flna* resulted in a marked increase in dendritic arborisation accompanied by modifications in spine morphology and distribution of mature excitatory synapses. We demonstrate that FLNA exerts its role in dendritogenesis by tuning RAC1 activation and cofilin phosphorylation through its interaction with the GTPase activating protein ARHGAP24 (also named as FilGAP). In fact, we show that overexpression of either the non-phosphorylable cofilin S3A mutant or the dominant-negative form of RAC1 or ARHGAP24 rescues the dendritic overgrowth induced by loss of *Flna*. Overall, our findings demonstrate a cell-autonomous role for FLNA in dendritic morphogenesis and spinogenesis, which are critical processes in the establishment of functional neuronal connectivity, thus probably contributing to pathogenesis of FLNA-related PNH.

2. Materials and methods

2.1. Animals

Breeding and experimental procedures were carried out in accordance with European guidelines (directive 86/609/EEC) for animal research and in accordance with French national institutional animal care guidelines (Authorization APAFIS#29902). *Flna*$^{flox/flox}$ (Flna$^{tm1.1Caw}$) and Nestin-Cre (B6.Cg-Tg(Nes-cre)1Kln/J) mice were obtained from Jackson Laboratories (Flna$^{tm1.1Caw}$: https://www.jax.org/strain/010907; Nestin-Cre: https://www.jax.org/strain/003771). The genetic background of both mice was C57BL/6. Mice were housed in ventilated, light-tight, sound-isolated chambers under standard 12:12 light/dark cycle (light on at 07.00 PM and light off at 07.00 AM) with food and water available *ad libitum*. The study was conducted in *Flna*$^{flox/flox}$ mice of both sexes unless otherwise specified.

2.2. In utero electoporation

Timed pregnant female *Flna*$^{flox/flox}$ mice at the E14 (E0 is counted as the morning on which the vaginal plug is detected) received buprenorphine (Buprecare, 0.045 mg/kg) and Carprofen (Rimadyl, 10 mg/kg) and were anaesthetized with sevoflurane (7.5% for induction and 3% for surgery). The uterine horns were exposed, and a lateral ventricle of each embryo was injected using pulled glass capillaries and a microinjector (PV 820 Pneumatic PicoPump; World Precision Instruments) with Fast Green (2 μg/ml; Sigma, USA) combined with the 1.5-3 μg of plasmid DNA constructs. Plasmids were further electroporated by delivering 30 V voltage pulses with a BTX ECM 830 electroporator (BTX Harvard Apparatus). The voltage was discharged in five electrical pulses at 950-ms intervals *via* 5-mm electrodes placed on the head of the embryo across the uterine wall.

2.3. Primary neuronal cultures and transfection

Primary cortical neurons were prepared from E18 brains of *Flna*$^{flox/flox}$ mice as previously described (Falace et al., 2014). Embryonic cortices were dissected and incubated in 0.125% trypsin (Gibco) for 25–30 min at 37 °C. Dissociated neurons were plated at low density (200 cells/mm^2), onto poly-L-lysine-coated 25 mm glass coverslips. Neurons were transfected with pCAG-GFP or pCAG-CRE and pCALNL-GFP at the day *in vitro* 3 by Lipofectamine 2000 (Thermo Fisher Scientific). Neurons were fixed 3 days post-transfection with 4% paraformaldehyde (PFA, Sigma-Aldrich) and 4% sucrose (Applichem) in 1× phosphate-buffered saline (PBS, Sigma Aldrich) at 37 °C for 15 min.

2.4. Expression constructs

ARHGAP24-full length; ARHGAPΔ648; RAC1T17N; RAC1-Q61L expression constructs were synthetised and cloned in the pCALNL-GFP using *Eco*RI and *Not*I restriction enzymes by Genescript (Piscataway, NJ). pEGFP-N1 human cofilin WT and pEGFP-N1 human cofilin S3A

were purchased from Addgene and subcloned into pCALNL-GFP constructs using EcoRI and NotI restriction enzymes. We performed Sanger sequencing of all constructs to confirm the correct insert orientation and validate their sequence.

2.5. Morphological analysis

2.5.1. Dendrites

Mice brains were perfused (P6 and P15) transcardially with Phosphate Buffered Saline (PBS), followed by 4% PFA and sliced at 100 μm on a vibratome (Microm). For morphometric analysis, images of GFP fluorescence were acquired on Olympus FluoView 300 confocal microscope. Images (50- to 70-μm-thick z-stacks) of isolated layer II/III pyramidal neurons and primary cortical neurons were acquired with a 40× oil-immersion objective, and *Z*-series were projected to 2D representations and used to sketch the neurite arbor. Quantification of dendritic length was performed after neuronal reconstructions with the ImageJ plug-in NeuronJ 1.2 software. A minimum of 65 neurons from at least 5 mice per condition were analysed and various parameters were evaluated and compared.

2.5.2. Spines

Flna$^{flox/flox}$ embryos were electroporated at E14.5 with either pCAG-EGFP or pCAG-Cre + pCALNL-GFP plasmids. Brains were collected at P15, sliced at 100 μm thickness with vibratome (Leica VT1000S) and imaged for GFP signal with confocal Olympus FluoviewFV500, 60× objective and 3× zoom factor (Z-stacks acquired at 1 μm step-size). Spine density and morphology of a secondary apical dendrites and a primary basal dendrite were analysed with the Neuronstudio 0.9.92 software (Rodriguez et al., 2008). Analyses were performed on maximal intensity projection images, not adjusted for brightness and contrast, and with default settings (X and Y voxel size set to 0.069 um). 5–10 images were analysed for each animal and mean spine densities and median morphological parameters were extrapolated.

2.5.3. Excitatory and inhibitory synapses

Imaging of P15 Flna$^{flox/flox}$ mice electoporated at E14.5 with FingR constructs (PSD95 or Gephyrin; 45) in combination either with pCALNL-dsRed and pCAG-CRE or pCAG-dsRed was done on Olympus FluoView 300 confocal microscope, 60× objective (Z-stacks acquired at 1 μm step-size). 40–80 cells from 5 pups for each condition were analysed for excitatory synapses; 50–109 cells from 5 to 6 pups for each condition were analysed for inhibitory synapses. Images were manually thresholded and PSD95 or Gephyrin puncta analysis was conducted in the selected dendritic region defined by dsRed fluorescence using ImageJ software.

2.6. Immunostaining

Electoporated P15 mice brains were perfused transcardially with Phosphate Buffered Saline (PBS), followed by 4% PFA and sliced at 100 μm on a vibratome (Microm). Slices were blocked at room temperature (RT) for 1 h with 5% normal goat serum and 0.3% Triton X-100 in PBS and incubated overnight at 37 °C with Tbr1 (Abcam; 1/4000), CDP (M-222 Santa Cruz Biotechnology; 1/200), Neu-N (Millipore; 1/300).

2.7. Active RAC1 pull-down assay

The activity of RAC1 was determined by the Active RAC1 Pull-Down and Detection Kit (Cytoskeleton, catalog no. BK035) according to the manufacture's procedure. The kit was used for the detection of RAC1 small GTPase activation through a GST-fusion protein containing the p21-binding domain (PBD) of human p21-activated protein kinase 1 (PAK1). Briefly, the total protein (at least 500 mg) extracted from cortical tissues of P15 *Flna*$^{Nestin\text{-}Cre+/y}$ hemizygote males and *Flna*$^{Nestin\text{-}Cre-/y}$ control males' tissues and an aliquot of the clarified supernatant was taken to test the total input of RAC1. The remainder was incubated with 10 μg GST-PAK1 PBD fusion protein bound to Glutathione-coupled agarose beads for 1 h at 4 °C. Subsequently, the beads were washed three times in cold Lysis Buffer, and bound proteins were eluted in 2× Laemmli reducing sample buffer. The eluted samples were heated for 5′, and then loaded onto SDS-PAGE gels for immunoblotting using mouse anti-RAC1 antibody (1:500; Cytoskeleton, #ARC03).

2.8. Western blot

Cortex tissues from mice were sonicated and lysed in RIPA buffer solution (Thermo Fisher Scientific) supplemented with protease and phosphatase inhibitor cocktails (Thermo Fisher Scientific). The protein concentration was determined using the BCA assay (Thermo Fisher Scientific). Proteins (100 μg) were run on a polyacrylamide gel (Blot 4–12% Bis-Tris, Invitrogen by Thermo Fisher Scientific) and transferred to a nitrocellulose membrane (GE Healthcare Life Science). Primary antibodies were incubated overnight at 4 °C and were as follows: alpha-tubulin (1:4000, Thermo Fisher Scientific, #62204); Cofilin (1:1000, Santa Cruz Biotechnology, #sc376476); phospho-cofilin (1:1000, Santa Cruz Biotechnology, #sc271921); S6 Ribosomal protein (1:500, Cell Signaling #2217), Phospho-S6 Ribosomal protein (1:500, Cell Signaling #2211) and Anti ADF/Destrin (1:1500, Thermo Fisher # PA1–24937). Signals were detected using substrate HR Immobilon Western reagent (MerckMillipore) and bands were analysed with ImageJ.

2.9. Statistical analysis

All statistical tests are described in the figure legends. Statistical methods to predetermine sample size were not used; sample sizes were estimated based on previous studies using the techniques described. Data are given as means ±SEM for *n* sample size. The normal distribution of experimental data was assessed using D'Agostino–Pearson's normality test. To compare two normally distributed sample groups, the two-tailed Student's *t*-test was used; otherwise, the Mann-Whitney's test was applied. To compare more than two normally distributed sample groups, one-way ANOVA, followed by Bonferroni's *post hoc* test, was used.

3. Results

3.1. FLNA regulates dendritic development of pyramidal neurons in vivo

To determine whether FLNA plays a specific role in dendritic complexity, we deleted *Flna* in a restricted population of neocortical neurons by timed *in utero* electroporation of Cre recombinase into developing conditional *Flna*$^{flox/flox}$ mouse ventricular zone (Fig. 1A). Ubiquitous Cre expression plasmid (CAG-Cre) was co-electroporated with the conditional loxP-STOP-loxP-GFP reporter plasmid (pCALNL-GFP) in neuroprogenitor cells by IUE at E14.5 to specifically target layer II-III pyramidal neurons. In this model, removal of conditional *Flna* allele (*Flna*^{cKO}) led to a migration delay in a highly restricted subset of developing neurons, whereas most of *Flna*^{cKO} neurons were correctly located in the cortical plate at E18 (Fig. S1). Such a defect was completely abolished when the Cre recombinase was expressed under the control of NeuroD1 promoter (*Flna*$^{cKO\text{-}ND1\text{-}Cre}$), which allows the selective removal of *Flna* in postmitotic neurons only (Aprea et al., 2014), thus suggesting that loss of FLNA protein might be dispensable for proper neuronal locomotion (Fig. S1). At postnatal day 6 (P6), all electroporated *Flna*^{cKO} neurons reached the cortical layer II/III (Fig. S2), leading us to investigate more deeply the consequence of FLNA loss at single cell level at this stage. Interestingly, *Flna*^{cKO} pyramidal neurons displayed a marked increase in their dendritic outgrowth and branching when compared with control neurons expressing GFP only (CAG-GFP) (Fig. 1A-C). This increase involved particularly the arborisation of the basal component (Fig. 1B-C). A similar even more pronounced increase

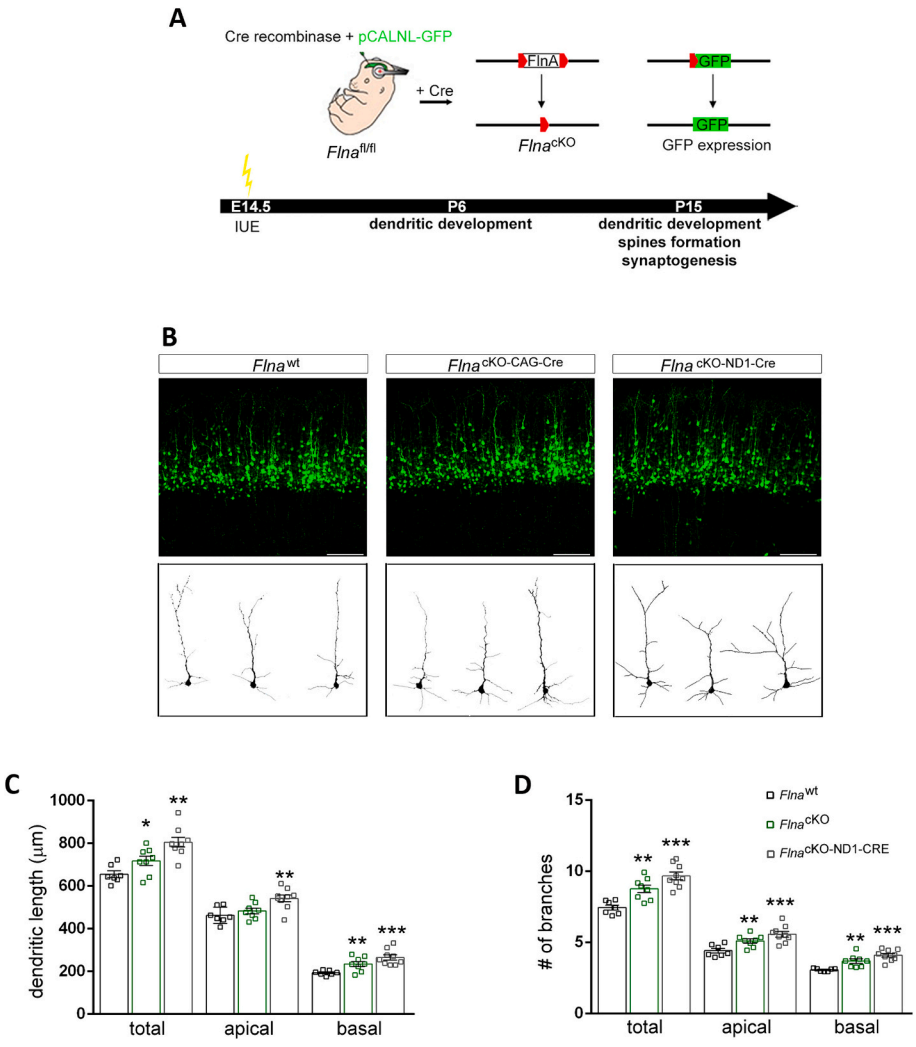

Fig. 1. Dendritic morphological analysis in P6 *Flna*^{cKO} neurons.
A) Schematic diagram of the experiments. Cre dependent removal of *Flna* was performed at E14.5 by IUE and properties of *Flna*^{cKO} neurons were analysed at postnatal stages P6 and P15. Concomitant GFP expression from pCALNL-GFP plasmid was used as Cre expression reporter. B) *Higher panels*, representative coronal sections of *Flna*$^{floxl/flox}$ P6 mouse brains electroporatedat E14.5 with GFP (*Flna*^{wt}) or pCALNL-GFP and pCAG-Cre (*Flna*^{cKO}) or NeuroD1-Cre (*Flna*$^{cKO\text{-}ND1\text{-}Cre}$) (scale bar, 100 µm). *Lower panels*, representative reconstructed layers II/III pyramidal neurons showing dendritic arborization patterns from the same experimental conditions shown in a. C—D) Quantification of total dendrite outgrowth (C) and number of processes (D) separated into apical and basal dendrites ($n = 7$ for *Flna*^{wt}; 11–32 neurons were reconstructed for each animal; $n = 8$ for *Flna*^{cKO}, 17–39 neurons were reconstructed for each animal; $n = 9$ for *Flna*$^{cKO\text{-}ND1\text{-}Cre}$, 12–30 neurons were reconstructed for each embryo). Data are means ±SEM and were compared *via* one-way ANOVA for repeated measures, followed by the Bonferroni's multiple comparison test. ***$P < 0.001$, **$P < 0.01$, *$P < 0.05$ *vs* *Flna*^{wt}.

in dendritic outgrowth was observed upon expression of Cre under the control of NeuroD1 promoter (*Flna*$^{cKO\text{-}ND1\text{-}Cre}$), which allows removal of *Flna* selectively in post-migrating neurons. Moreover, dendritic overgrowth was also observed in Cre-transfected *Flna*^{cKO} cortical cultured neurons (Fig. S3), further confirming the cell-autonomous function of FLNA in regulating dendritic complexity.

At P15, we found that dendritic overgrowth is an established feature of *Flna*^{cKO} neurons, clearly involving at this stage both apical and basal compartments (Fig. 2). In addition, *Flna*^{cKO} neurons displayed more developed primary basal processes with longer and supernumerary secondary branches (Fig. 2D-E**).**

3.2. Loss of FLNA affects dendritic spine distribution and morphology

Dynamic remodeling of the actin cytoskeleton provides the driving force behind structural alterations underlying dendritic spine formation and morphological maturation, a process tightly associated with synaptic strength, with larger spines – ranging from so-called mushroom to thin spines - representing stronger synapses, and short and wide immature spines (defined as "stubby") typically appearing during early synaptogenesis (de Curtis, 2008; Penzes et al., 2008; Costa et al., 2020). In addition, FLNA protein levels have been shown to be critical for dendritic spine regression associated with hypoxia *in vitro* (Segura et al., 2016). We wondered whether the loss of FLNA could affect the formation of dendritic spines *in vivo*. To address this question, we analysed dendritic spine density and morphology in apical and basal secondary dendritic branching of P15 *Flna*^{cKO} cortical pyramidal neurons by using GFP as a morphology and transfection marker. The analysis revealed that the density of the spines was significatively reduced in both apical and basal secondary branches in P15 *Flna*^{cKO} neurons compared to isochronic *Flna*^{wt} controls (Fig. 3A-C). Next, to determine whether loss of FLNA expression altered the distribution of spine type, we categorized spines into stubby, thin and mushroom, and determined the density, the length and the head diameter of each spine type per dendrite. We found that loss of FLNA strongly reduced the density of the mushroom spines in apical and basal dendrites whereas the density of stubby and thin spines

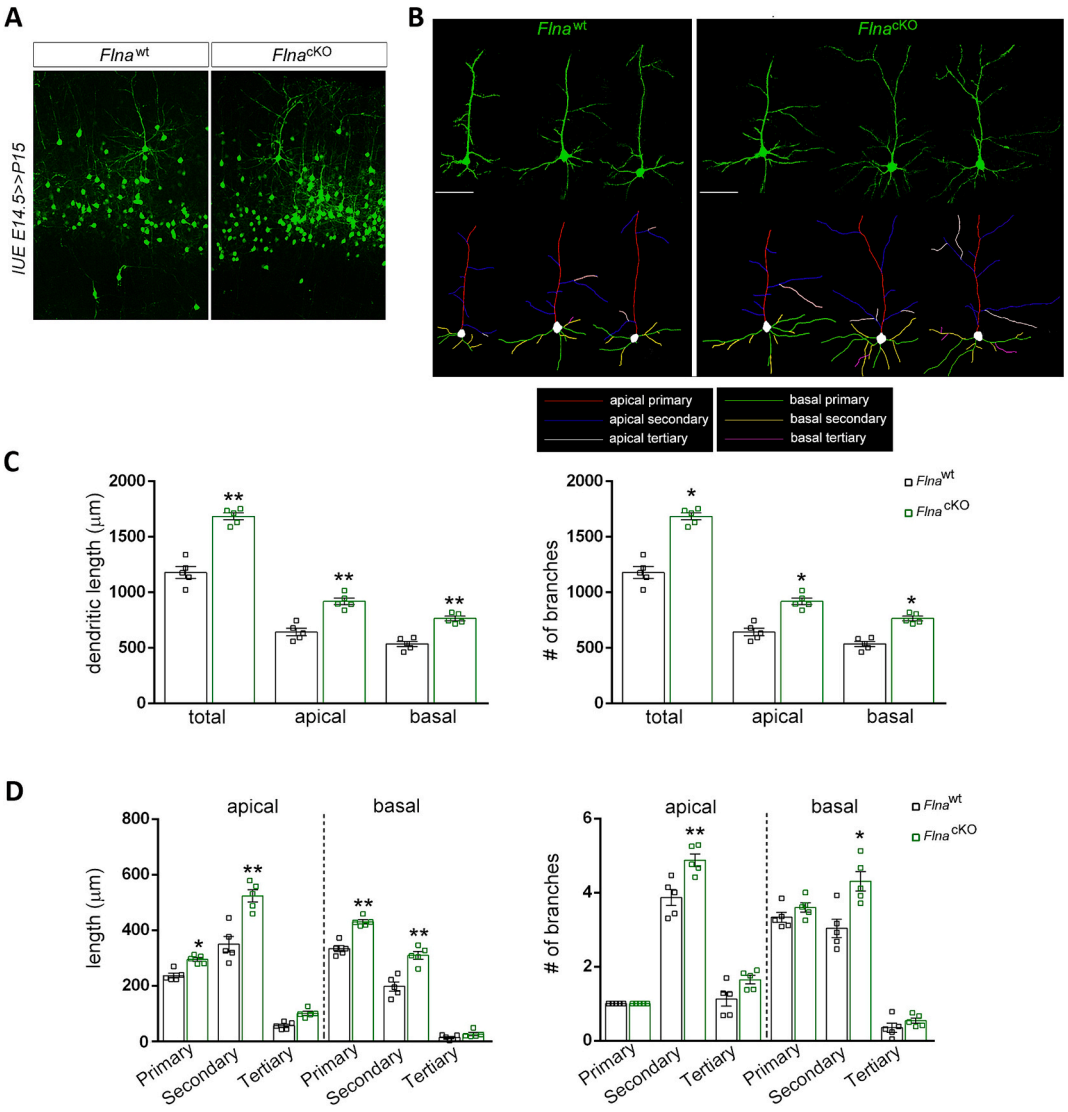

Fig. 2. *In vivo* morphological analysis of *Flna*^{cKO} cortical neurons at P15. A). Representative coronal sections of P15 mouse *Flna*$^{flox/flox}$ brains transfected by IUE at E14.5 with GFP (*Flna*^{wt}) or with pCALNL-GFP and pCAG-CRE (*Flna*^{cKO}) (scale bar, 100 μm). B) *higher panels*, high magnification images of layer 2/3 cortical neurons from the same experimental condition shown in b (scale bar, 50 μm). *Lower panels*, "skeleton outline" of basal and apical arbours, separated into primary, secondary, and tertiary branches, of neurons shown in B. C—D) Quantification of dendrite outgrowth length (left panels) and number of processes (right panels) separated into apical/basal, primary/secondary/tertiary order branches. *Flna*^{cKO} *in vivo* enhances both apical and basal arbours outgrowth, specifically driven by an increase in the complexity of primary and secondary order branches ($n = 5$ for *Flna*^{wt}, 13–23 reconstructed neurons for each animal; n = 5 for *Flna*^{cKO}, 12–21 reconstructed neurons for each animal). Data are means ±SEM and were analysed by unpaired two-tailed *t*-test (**P < 0.01, *P < 0.05).

was unaffected (Fig. 3D and G). The head diameter of apical stubby spines and – to a lesser extent – mushroom spines of *Flna*^{cKO} neurons were also decreased (Fig. 3E and H). Moreover, we observed that the spine length was barely reduced in mushroom type of apical dendrites as well as in thin spine type of basal dendrites (Fig. 3F and I). These data reveal that depletion of FLNA alters dendritic spine distribution and maturation along the dendritic arbours. Combined to the herein observed role of FLNA in dendritic outgrowth, these findings reveal the relevant role of FLNA in the dynamic processes that tightly coordinate morphological development and functional maturation of the cortical networks.

3.3. Unbalance between excitatory and inhibitory synapses in *Flna*^{cKO} neurons

In rodents' brains active synaptogenesis and synapse maturation peak around two weeks. At this developmental stage, neurons establish complex connectivity and form functional networks by balancing excitatory and inhibitory inputs. To investigate the role of FLNA in synaptogenesis, we assessed alterations of synapses *in vivo* using recombinant probes that allow the visualization of excitatory and inhibitory synapses formed by developing neurons (Gross et al., 2013). For this purpose, we electroporated E14.5 *Flna*^{cKO} embryos with pCALNL-dsRed and pCAG-CRE or pCAG-dsRed in combination with FingR-PSD95 or FingR-Gephyrin plasmids to label endogenous excitatory synapses and inhibitory contacts, respectively. Pyramidal neurons were then analysed at P15. At this stage, we found that the density of PSD95-positive excitatory contacts was reduced in both apical and basal compartments of the *Flna*^{cKO} neurons when compared to control neurons, accordingly and similarly to spine density reduction observed in isochronic *Flna*^{cKO} neurons (Fig. 4A-B). In contrast, the density of Gephyrin-positive inhibitory synaptic contacts in both apical and basal dendrites was not significantly different in *Flna*^{cKO} and control P15 neurons (Fig. 4C-D). These results unveil a prominent role of FLNA in excitatory synaptogenesis and suggest that loss of FLNA could finally lead to an unbalance between excitatory and inhibitory inputs in the

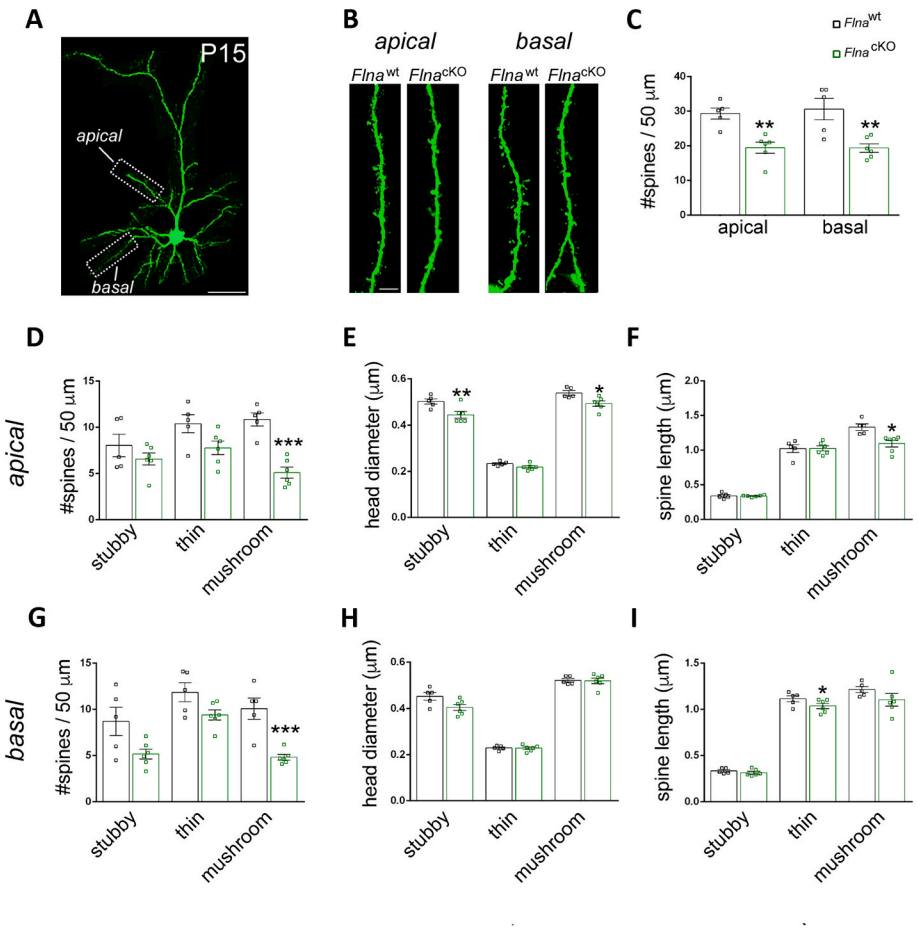

Fig. 3. Dendritic spines density and morphology alterations in *Flna*^{cKO} neurons. A) Representative image of a neuron electroporated at E14.5 and integrated in layer 2/3 of the somatosensory cortex at P15 (scale bar, 50 µm). Apical oblique and basal dendrites were selected for the analysis as indicated in dashed boxes. B) High-magnification images of apical oblique and basal dendritic segments of *Flna*^{wt} and *Flna*^{cKO} neurons (scale bar, 5 µm). C) Quantitative analysis of total spine density in apical oblique and basal dendrites in *Flna*^{wt} and *Flna*^{cKO} neurons (n = 5 for *Flna*^{wt}, *n* = 6 for *Flna*^{cKO}, 5–10 apical and basal dendrites for each animal). D and G) Quantitative analysis of stubby, thin and mushroom subset spine density in apical oblique and basal dendrites in *Flna*^{wt} and *Flna*^{cKO} neurons (n = 5 for *Flna*^{wt}, n = 6 for *Flna*^{cKO}, 5–10 apical and basal dendrites for each animal. E, F, H and I) Quantitative analysis of stubby, thin and mushroom morphological parameters (E and H head diameter; F and I spine length) in apical oblique and basal dendrites in *Flna*^{wt} and *Flna*^{cKO} neurons (n = 5 for *Flna*^{wt} n = 6 for *Flna*^{cKO}, 5–10 apical and basal dendrites for each animal. Data are expressed as mean ± SEM and were analysed by unpaired two-tailed t-test (***$p < 0.001$, **$p < 0.01$, *$p < 0.05$).

cortical network.

3.4. FLNA regulates dendritic growth by modulating cofilin activation

FLNA has been shown to modulate actin dynamics by regulating the function of the small GTPase RAC1 (Ohta et al., 2006), which coordinates several aspects of neuronal development including the establishment of neuronal polarity, neurite branching and synapse formation (de Curtis, 2008). Active GTP-bound RAC1 triggers a cascade resulting in the phosphorylation/inactivation of the actin-depolymerizing factor ADF/cofilin, thus leading to the stabilization of the actin cytoskeleton (Bokoch, 2003; Llano et al., 2015). Therefore, to assess whether cofilin activity dysregulation underlies the dendritic abnormalities observed in the *Flna*^{cKO} model we tested the levels of phosphorylated, inactive, cofilin (p-cofilin) in cortical brain tissues lacking *Flna*. For this purpose, we crossed the *Flna*^{cKO} female mice with a *Nestin*-Cre transgenic male mouse to drive selective *Flna* deletion in the central nervous system. Total levels of cofilin and p-cofilin were analysed by Western blot in *Flna*$^{Nestin\text{-}Cre+/y}$ hemizygote males and *Flna*$^{Nestin\text{-}Cre-/y}$ control males from the same litters. Total cofilin abundance did not differ significantly in *Flna*$^{Nestin\text{-}Cre+/y}$ mice *versus* controls, whereas phosphorylated cofilin was significatively increased in cortical lysates lacking *Flna* (Fig. 5A). Consistently, we assessed whether elevated cofilin phosphorylation may give rise to abnormal dendritic growth. For this purpose, we analysed the *in vivo* effect of constitutively active non-phosphorylatable form of cofilin (cofilinS3A) in *Flna* depleted neurons. As *in vivo* overexpression of CofilinS3A, under the CAG promoter, impairs neuronal migration (Chai et al., 2016; Fig. S4), we created a Cre-inducible CofilinS3A to express it by *in utero* electroporation selectively in postmitotic *Flna*$^{cKO\text{-}ND1\text{-}Cre}$ neurons (Fig. S4). At P6, we found that overexpression of CofilinS3A mutant in *Flna* knockout neurons restored dendritic outgrowth and complexity to physiological levels (Fig. 5B-D). Taken together, these results suggest that FLNA may play a pivotal role in modulating cofilin activity to promote dendritogenesis.

3.5. FLNA modulates RAC1-cofilin activity through its interaction with ARHGAP24

Modulation of cofilin phosphorylation mainly relies on RAC1 activation, (Yang et al., 1998; Edwards et al., 1999), we therefore assessed the endogenous levels of GTP-bound (active) Rac1 in *Flna* knockout brains. We found that Rac1-GTP was increased in the cortex of *Flna*$^{Nestin\text{-}Cre+/y}$ hemizygote males relative to *Flna*$^{Nestin\text{-}Cre-/y}$ control males, with little or no detectable difference in total Rac1 abundance (Fig. S5). Next, we wondered whether lowering the levels of active RAC1 *in vivo* prevented the dendritic overgrowth observed in *Flna*^{cKO} neurons. To

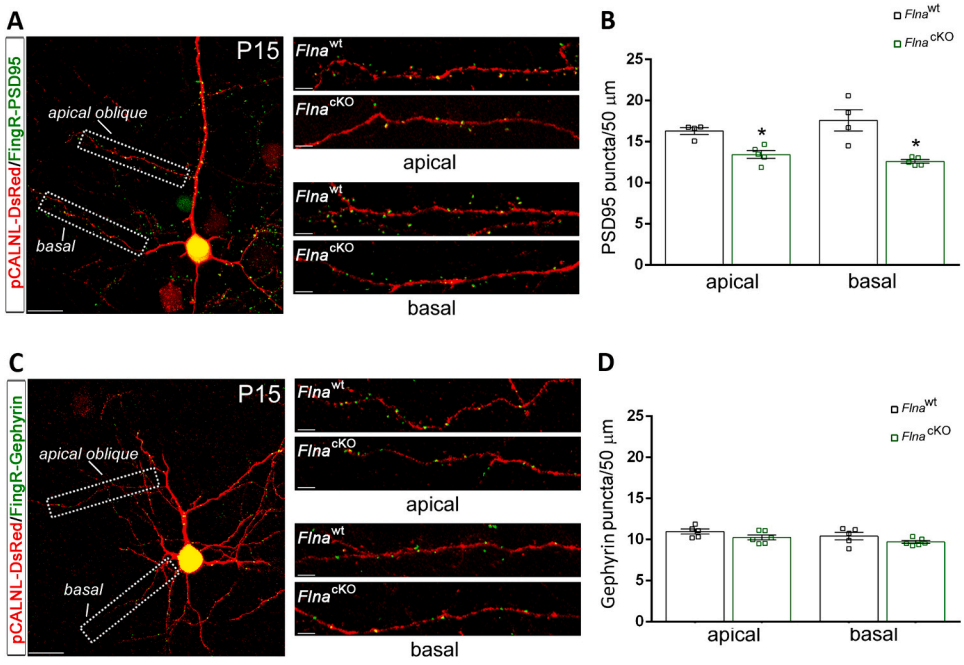

Fig. 4. Distribution of excitatory and inhibitory postsynaptic inputs in *Flna*^{cKO} cortical pyramidal neurons. A and C) Representative image of layer 2/3 *Flna*$^{flox/flox}$ neuron of the somatosensory cortex at P15 electroporated with pCAG-CRE, pCALNL-dsRed combined with FingR-PSD95 (A) or FingR-Gephyrin (C) constructs (scale bar, 80 µm). *Flna*$^{flox/flox}$ electroporated with pCAG-dsRed combined with FingR-PSD95 or FingR-Gephyrin constructs were used as controls. High-magnification images on apical and basal dendritic tracts of *Flna*^{wt} and *Flna*^{cKO} P15 cortical neurons were shown on the right (scale bar, 5 µm). B and D) Quantitative analysis of the PSD95 (B) or Gephyrin (D) puncta density in apical and basal dendritic compartments. Individual data and means ±SEM are shown. (PSD95: 40–51 apical and basal dendrites from 4 animals for *Flna*^{wt}; 68–80 apical and basal dendrites from 5 animals for *Flna*^{cKO}. Gephyrin: 50–66 apical and basal dendrites from 5 animals for *Flna*^{wt}; 65–109 apical and basal dendrites from 6 animals for *Flna*^{cKO}; *P < 0.05 unpaired two-tailed t-test).

directly test this issue, we altered *in vivo* the activity of RAC1 in *Flna* depleted neurons by overexpressing the RAC1-GDP inactive form (RAC1-T17N) (Fig. 6A) (Chai et al., 2016). As RAC1 dysfunction has been reported to disrupt neuronal migration (Tahirovic et al., 2010) (Fig. S6), henceforth experiments were performed in *Flna*$^{cKO\text{-}ND1\text{-}Cre}$ neurons. We found that *Flna*$^{cKO\text{-}ND1\text{-}Cre}$ cells overexpressing the constitutively inactive RAC1-T17N displayed a significant reduction in the size and number of both apical and basal dendrites when compared to *Flna*$^{cKO\text{-}ND1\text{-}Cre}$ neurons (Fig. 6B-D). In contrast, the overexpression of the constitutively active RAC1 (RAC1Q61L) enhanced dendritic overgrowth of *Flna*$^{cKO\text{-}ND1\text{-}Cre}$ neurons (Fig. S7), suggesting that FLNA protein controls cofilin phosphorylation by regulating levels of active RAC1 *in vivo*. In non-neuronal cells, FLNA interacts with ARHGAP24 (or FilGAP), a RAC1-GTPase-activating protein (GAP) and targets it to sites of membrane protrusion where it inactivates RAC1 signaling (Ohta et al., 2006) (Fig. 6A). In addition, it has been shown that ARHGAP24 decreased neurite outgrowth in cultured neurons (Nguyen et al., 2012). Accordingly, overexpression of ARHGAP24 in the developing cortex by IUE decreased neuronal dendritic outgrowth *in vivo* when compared to control isochronic neurons (Fig. S8). In contrast electroporation of the ARHGAP24Δ648 truncated form lacking the FLNA binding domain (14, 36) did not impair dendritic outgrowth further suggesting that ARHGAP24 exerts its role on RAC1-GTP levels by interacting with the FLNA protein.

Therefore, we wondered whether lowering the levels of active RAC1 *in vivo* through ARHGAP24 overexpression prevented the dendritic overgrowth observed in *Flna* depleted neurons. Remarkably, in P6 *Flna*$^{cKO\text{-}ND1\text{-}Cre}$ neurons overexpressing ARHGAP24, the length and arborization of apical and basal dendrites were strikingly reduced compared to *Flna*$^{cKO\text{-}ND1\text{-}Cre}$ neurons and did not significantly differ from isochronic *Flna*^{wt} neurons (Fig. 6B-D), suggesting the FLNA/ARHGAP24 binding is needed to maintain physiological levels of active RAC1 and, therefore, for a proper dendritogenesis in cortical neurons.

4. Discussion

In this study we demonstrated that loss of FLNA protein in developing cortical neurons resulted in a marked overgrowth of the dendritic tree accompanied by a profound reorganization of dendritic spines and synaptic contacts.

A proper dendritic growth is critical for neuronal function, as the size and shape of the dendritic arborization define the neuron's receptive field that is crucial for its functional connectivity. According to this, abnormal dendritic complexity is a shared feature of many neurodevelopmental disorders associated with neurological defects (Jan and Jan, 2010; Nestor and Hoffman, 2012; Nelson and Bender, 2021). *In vivo* cell autonomous FLNA depletion resulted in a hypertrophic dendritic tree in mouse cortical neurons compared to cells expressing normal FLNA protein levels. Such a defect was already visible in the first postnatal stages of the dendritic development and became more evident at P15, suggesting that dendritic overgrowth is a feature of *Flna*^{cKO} neurons. Removal of *Flna* in cortical cultured neurons also promoted neurite overgrowth confirming the cell autonomous role for FLNA protein in neuronal dendritogenesis. Expression of FLNA protein peaks around birth in rodents' brains (Sheen et al., 2002; Carabalona et al., 2012) but is maintained at postnatal stages when morpho-functional maturation of cortical neurons occurs (Noam et al., 2012), further suggesting a neurobiological role of FLNA in later neuronal development.

It has been shown in wild-type olfactory bulb granule cells that both under- and over-expression of FLNA protein led to more complex dendritic arborization *in vivo* (Zhang et al., 2014). Increased FLNA levels in the *Tsc1*^{null} mice due to MEK-ERK1/2 hyperactivation led to dendritic overgrowth and restoring appropriate levels of FLNA normalized dendritic growth and synaptic activity (Zhang et al., 2014). The TSC complex represses the Ras homolog enriched in brain (Rheb) activity, the canonical activator of mTOR complex1 (mTORC1). Thus, *Tsc1*-loss leads to hyperactive mTORC1 and consequent phosphorylation of rpS6 in

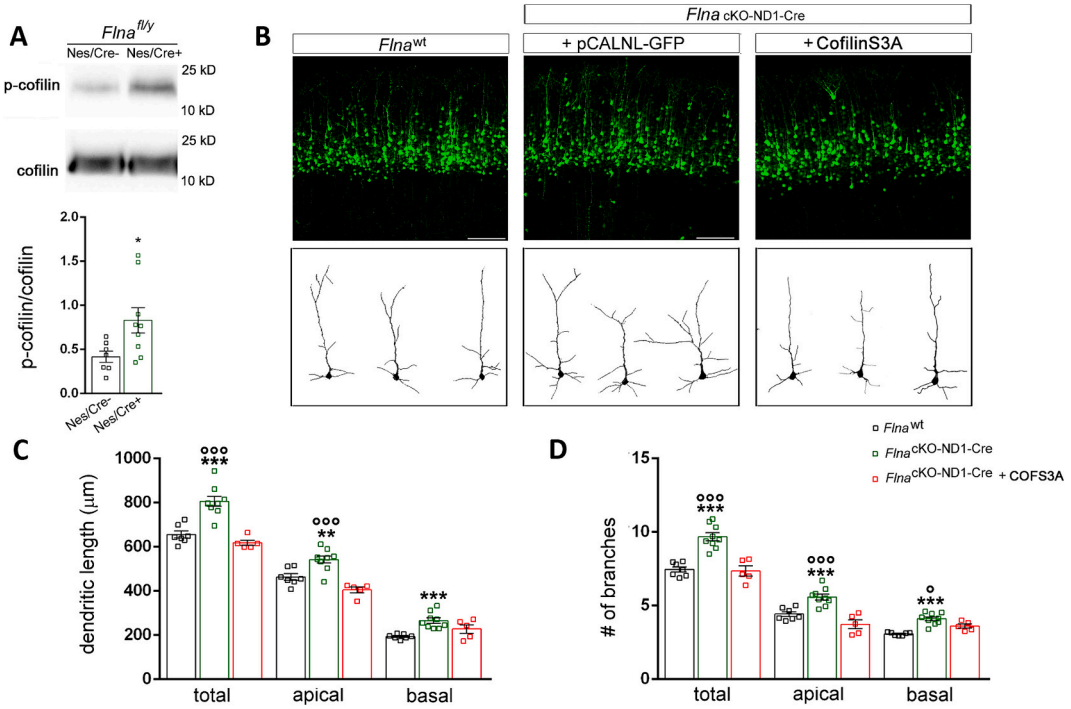

Fig. 5. Dysregualtion of Cofilin phosphorylation underlies dendritic overgrowth in Flna$^{cKO\text{-}ND1\text{-}Cre}$ cortical neurons. A) Representative western blot (top) and summary data (bottom) assessing the abundance of phosphorylated (p-) and total cofilin in brain lysates from P15 cortex of *Flna*$^{Nestin\text{-}Cre+/y}$ hemizygote males (Nes/Cre+) and *Flna*$^{Nestin\text{-}Cre-/y}$ control males (Nes/Cre-). Data are means ±SEM and were analysed by paired two-tailed *t*-test. *$P < 0.05$. *Flna*$^{Nestin\text{-}Cre-/y}$ n = 7; *Flna*$^{Nestin\text{-}Cre+/y}$ $n = 9$. B) *Higher panels*, representative coronal sections of P6 *Flna*$^{flox/flox}$ mouse brains electoporated at E14.5 with GFP (*Flna*^{wt}) or pCALNL-GFP + NeuroD1-CRE (*Flna*$^{cKO\text{-}ND1\text{-}Cre}$) alone (pCALNL-GFP) or in combination with pCALNL-CofilinS3A (CofilinS3A) (scale bar, 100 μm). *Lower panels*, representative reconstructed layers II/III pyramidal neurons showing dendritic arborization patterns from the same experimental conditions shown above. C—D) Quantification of total dendritic outgrowth (C) and number of processes (D) separated into apical and basal dendrites (n = 7 for *Flna*^{wt}; 11–32 neurons were reconstructed for each animal;n = 9 for *Flna*$^{cKO\text{-}ND1\text{-}Cre}$, 12–30 reconstructed neurons for each animal; n = 6 for *Flna*$^{cKO\text{-}ND1\text{-}Cre}$ + Cofilin S3A, 6–9 reconstructed neurons for each animal). Data are means ±SEM were compared *via* one-way ANOVA for repeated measures, followed by the Bonferroni's multiple comparison test (***P < 0.001, **P < 0.01, *vs* *Flna*^{wt}; ◦◦◦P < 0.001, ◦P < 0.05 *vs* *Flna*$^{cKO\text{-}ND1\text{-}Cre}$; *Flna*$^{cKO\text{-}ND1\text{-}Cre}$ + Cofilin S3A).

neurons (Zhang et al., 2014; Zhang et al., 2020). In *Flna*$^{Nestin\text{-}Cre+/y}$ mouse model cortical levels of phosphorylated rpS6 did not differ compared to control samples suggesting that FLNA acts downstream of the mTOR pathway (Fig. S9). Thus, modulation of FLNA activity could represent an ideal end target for the regulation of actin dynamics through RAC1-to-cofilin and different convergent pathways could impinge on FLNA.

Previous findings suggested a role for FLNA protein at synaptic sites (Segura et al., 2016; Jobin et al., 2023). Accordingly, we reported that FLNA loss affects dendritic spine distribution and morphological maturation in cortical *Flna*^{cKO} neurons that migrate normally in normotopic cortex, and which represent the majority (90%) of *Flna* deficient neurons. This defect was accompanied by a concomitant decrease in the excitatory synaptic contacts established by *Flna*^{cKO} neurons whereas inhibitory synapse distribution was unchanged. Notably, putative total spines number *per* cell is not significatively changed in *Flna*^{cKO} neurons compared to control neurons (Fig. S10). Spine density reduction in secondary branches of *Flna*^{cKO} neurons could be either attributable to a direct role of FLNA in dendritic spine formation and stabilization, or it might represent an active feedback mechanism by which *Flna*^{cKO} neurons eventually compensate for dendritic overgrowth. Further studies are needed to assess the global consequences of FLNA-related defects on neuronal excitability and synaptic transmission in *Flna*^{cKO} neuronal circuits.

Our data demonstrate that the increased neuronal complexity in *Flna*^{cKO} excitatory cortical neurons reflects a dysregulation of the activity of the RAC1 GTPase, a key determinant in actin dynamics. In non-neuronal cells, ARHGAP24 GAP activity on RAC1 is modulated by phosphorylation and by binding to FLNA, which ultimately impacts the phosphorylation state of the actin severing enzyme cofilin (Ohta et al., 2006; Nakamura, 2013). The fine tuning of RAC1 is essential to determine the rate and size of dendritic outgrowth (de Curtis, 2008). Accordingly, the expression of a dominant-negative RAC1 in wild-type cortical neurons caused a marked reduction in the number of primary dendrites. Conversely, the expression of constitutively active RAC1 led to an increase in the number of primary and basal dendrites *in vitro* (de Curtis, 2008; Threadgill et al., 1997). These new results are consistent with the observation that the genetic deletion of RAC1 regulatory proteins results in neuritogenesis alterations and hyperphosphorylation of cofilin accompanied by dysregulation of PAK-LIMK pathway (Xiang et al., 2016; Zamboni et al., 2018). Accordingly, the expression of constitutively non-phosphorilable cofilin restores physiological levels of dendritic outgrowth in *Flna* depleted neurons and further corroborated the relevance of a FLNA-RAC1-Cofilin regulatory axis in dendritogenesis.

In this study, we showed that FLNA modulates ARHGAP24 activity on RAC1 in cortical neurons *in vivo*. Overexpression of ARHGAP24 or of the dominant-negative form of RAC1 rescues the dendritic overgrowth induced by embryonic loss of *Flna* gene. *In utero* overexpression of ARHGAP24 alone in a wild-type cerebral cortex also resulted in abnormal dendritic outgrowth whereas removal of FLNA-binding domain (ARHGAP24Δ648) prevented this phenotype, thus demonstrating that FLNA represents an upstream modulator of ARHGAP24-RAC1-cofilin pathway. However, we cannot exclude that FLNA may modulates cofilin activity also through mechanisms alternative to RAC1. Indeed, the interplay between RhoA and RAC1 is a major determinant of cofilin activation through PAK1. It has been shown that FLNA interact with RhoA in brain tissues (Lian et al., 2019), but the impact of FLNA-

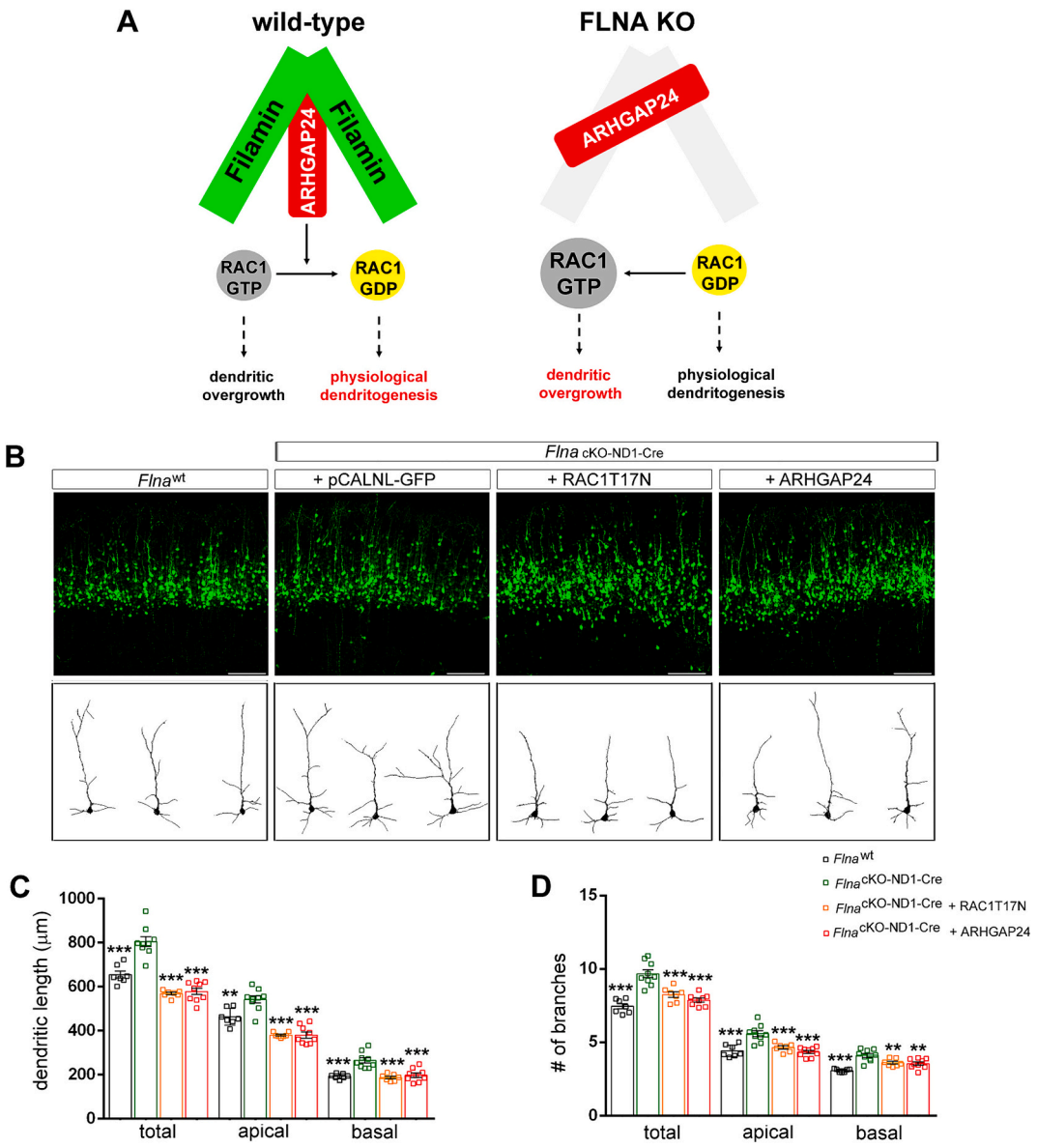

Fig. 6. *In vivo* lowering of RAC1-GTP or overexpression of ARHGAP24 in *Flna*$^{cKO\text{-}ND1\text{-}Cre}$ neurons prevents dendritic overgrowth. A) Schematic diagram of the FLNA/ARHGAP24/RAC1 functional interaction. FLNA binding targets ARHGAP24 to sites of membrane protrusion, where it antagonizes RAC1, a small GTPase that cycles between inactive GDP-bound and active GTP-bound forms. ARHGAP24 accelerates GTP hydrolysis, thereby inactivating RAC1. B) *Higher panels*, representative coronal sections of P6 *Flna*$^{flox/flox}$ mouse brains electoporated at E14.5 with GFP (*Flna*^{wt}) or pCALNL-GFP + NeuroD1-CRE (*Flna*^{cKO}) alone or in combination with pCALNL-RAC1T17N (*Flna*$^{cKO\text{-}ND1\text{-}Cre}$ + RAC1T17N) or pCALNL-ARHGAP24 (*Flna*$^{cKO\text{-}ND1\text{-}Cre}$ + ARHGAP24) (scale bar, 100 µm). *Lower panels*, representative reconstructed layers II/III pyramidal neurons showing dendritic arborization patterns from the same experimental conditions shown above. C, D) Quantification of total dendritic outgrowth (C) and number of processes (D) separated into apical and basal dendrites (n = 7 for *Flna*^{wt}; 11–32 neurons were reconstructed for each animal;n = 9 for *Flna*$^{cKO\text{-}ND1\text{-}Cre}$, 12–30 reconstructed neurons for each animal; n = 7 for *Flna*$^{cKO\text{-}ND1\text{-}Cre}$ + RAC1T17N, 18–28 reconstructed neurons for each animal; n = 9 for Flna$^{cKO\text{-}ND1\text{-}Cre}$ + ARHGAP24,17–27 reconstructed neurons for each animal). Data are means ±SEM were compared *via* one-way ANOVA for repeated measures (***P < 0.001, **P < 0.01, * *Flna*$^{cKO\text{-}ND1\text{-}Cre}$).

RHOA in cofilin activity has not been investigated. Ours rescue experiments on dendritogeneiss using constitutively inactive RAC1 or ARHGAP24, which displays a specific GAP activity toward RAC1, support a pivotal role of FLNA-RAC1 complex on cofinlin activity.

Actin is the most abundant cytoskeletal protein in dendritic spines (Cingolani and Goda, 2008; Hotulainen and Hoogenraad, 2010), and modulation of actin polymerization/depolymerization balance determines spine morphogenesis, synaptogenesis and synaptic plasticity (Minegishi et al., 2023). The actin-depolymerizing enzymes of the ADF/cofilin family represents the endpoint factor that regulates dendritic spine dynamics, as severing of F-actin allows spine maturation. Upon phosphorylation mediated by PAK1 on specific residues (Bamburg et al., 2021), cofilin turns into an inactive state leading to actin stabilization. Increased levels of cofilin phosphorylation in *Flna*$^{Nestin\text{-}Cre+/y}$ cortices indicate that p-cofilin/cofilin unbalance contribute to synaptic defects identified in the *Flna*^{cKO} model (schematic diagram of the proposed molecular mechanism is shown in Fig. S11). In addition, in *Flna* knockout cortex total levels of ADF were unchanged (Fig. S12), suggesting that increased cofilin phosphorylation may be not functionally compensated. Cofilin inactivation has been extensively shown to enhance spine maturation and stabilization (Bamburg et al., 2021; Rust, 2015). In *Flna* depleted cells dendritic hypertrophy was accompanied by cofilin inactivation and altered distribution of spines. In addition, we found a reduction of the relative frequency of mushroom spines but no

changes in their putative total number (Fig. 3 and Fig. S10). A possible explanation for this discrepancy may engage the intrinsic role of FLNA on actin stability at spines. The spine head contains a dense network of branched F-actin filaments, which decrease in density toward the head-neck junction (Korobova and Svitkina, 2010; Bär et al., 2016). As FLNA is an essential F-actin-crosslinking protein, loss of *Flna* may hinder the formation of F-actin network at the spine head thus preventing the formation of mature mushroom spines. Indeed, tight regulation of FLNA levels is required for the proper dendritic spine formation *in vitro* (Segura et al., 2016), but the molecular mechanism remains unknown. Our findings indicate that loss of FLNA at the dendritic spines could hinder spine maturation independently from cofilin phosphorilation, suggesting a dual role of the FLNA-Cofilin interplay on actin network remodeling either at the dendrites and/or at spines. Additional studies at earlier and later developmental stages are required to provide a clearer picture on the FLNA function in spines development and function. Ideally, such analysis should combine live imaging of spines dynamics with single-cell electrophysiological recordings, which represents an essential readout to determine the maturation rate of dendritic spines.

It is important to note that altered RAC1 activity in excitatory and inhibitory brain circuits results in excitability unbalance (Hotulainen and Hoogenraad, 2010), and dysfunctions in RAC1-to-cofilin signaling have been related to several brain diseases ranging from early-onset developmental disorders, psychiatric conditions (major depressive disorder) to neurodegenerative disorders. For instance, stress-induced decreases in RAC1 expression have been shown to impair spines maturation by promoting the selective increase of cofilin-positive immature stubby spines (Golden et al., 2013). Interestingly, restoring appropriate levels of RAC1-to-cofilin signaling represents a potential therapeutic option. Indeed, correction of aberrantly increased RAC1 activity corrects aberrant spine defects in the somatosensory cortex of the X-fragile mouse model (*Fmr1* KO) (Pyronneau et al., 2017) and rescues the social deficits in the *Shank3B* knockout mouse model of autism (Ma et al., 2022). *De novo* mutations in RAC1 have been identified in variable combinations of developmental delay, intellectual disability and brain anomalies such as polymicrogyria (Reijnders et al., 2017; Banka et al., 2022). However, the direct contribution of downstream effects of RAC1 dysregulation on cofilin function has not been investigated in these patients.

Neuropsychiatric presentations are an often-underestimated consequence of *FLNA*-patients (Fry et al., 2013) and *de novo* variants in *FLNA* associated with autism have been found (Wegiel et al., 2010; Gilman et al., 2011).

Morpho-functional maturation abnormalities associated with FLNA-loss in cortical pyramidal neurons strongly support the idea that a wide and extensive neural circuit dysfunction underlies *FLNA* mutations. Our findings corroborate the hypothesis that heterotopic nodules could represent a hallmark of a more global cortical network dysfunction in patients. Grey matter heterotopia may reflect early-stage dysfunction on neurodevelopmental steps whose real extent become evident later on cortical excitability. Accordingly, *FLNA*-patients develop seizures regardless of PNH presence (Wei et al., 2018; Hiromoto et al., 2020). In the *in utero Flna*-model we can appreciate transient and embryonic restricted neuronal migration defects. Such phenotype, which involved a low fraction of migrating neurons, was even less evident at postnatal stages. Interestingly, selective removal of *Flna* in postmitotic neurons did not affect cortical migration. Electrophysiological studies on CAG-CRE *versus* NeuroD1-CRE electoporated $Flna^{cKO}$ neurons will rule out whether the initial migration delay impacts on cortical network function or not. However, the absence of ectopic nodules also in the two *Flna* knockout mice strains that have been developed so far (Feng et al., 2006; Hart et al., 2006), suggest caution in considering the mouse brain lacking *Flna* as a faultless model for the study of the FLNA role in the human brain.

Epileptic seizures represent the most common neurological manifestation in PNH patients harbouring *FLNA* mutations, but the epileptic foci could involve ectopic neurons, normotopic cortex or both (Pizzo et al., 2017). Further key evidence about FLNA involvement in epileptogenesis came from Zhang and colleagues, who showed that downregulation of FLNA prevents seizures in a mouse model of focal cortical dysplasia (FCD) (Zhang et al., 2020). Indeed, the expression of FLNA was found to be increased in cortical foci resected from patients with FCD type II as well in rodent FCD models, and downregulating FLNA with either RNA interference or the small molecule PTI-125 reduced seizure frequency (Zhang et al., 2020). However, the molecular mechanisms through which FLNA promotes neuronal hyperexcitability still remain unknown.

To conclude, our present data show the role of FLNA in the development of cortical networks and have identified some of the molecular partners with which it influences dendritic maturation and synaptogenesis. Our data indicate that FLNA loss of function, beyond PNH genesis, significantly disrupts the development of the normotopic cortex. These changes could provide a pathophysiological substrate for the neuropathological disorders associated with *FLNA* mutations.

CRediT authorship contribution statement

Antonio Falace: Writing – review & editing, Writing – original draft, Visualization, Validation, Supervision, Methodology, Investigation, Formal analysis, Data curation, Conceptualization. **Lea Corbieres:** Investigation, Formal analysis, Data curation. **Catia Palminha:** Investigation, Formal analysis, Data curation. **Fabrizia Claudia Guarnieri:** Methodology, Investigation, Formal analysis, Data curation. **Fabienne Schaller:** Investigation. **Emmanuelle Buhler:** Investigation. **Clara Tuccari di San Carlo:** Data curation. **Aurelie Montheil:** Investigation. **Françoise Watrin:** Formal analysis. **Jean Bernard Manent:** Formal analysis. **Alfonso Represa:** Writing – original draft, Visualization. **Antoine de Chevigny:** Writing – original draft, Visualization. **Emilie Pallesi-Pocachard:** Methodology, Investigation, Formal analysis, Data curation. **Carlos Cardoso:** Writing – review & editing, Writing – original draft, Visualization, Validation, Supervision, Resources, Project administration, Funding acquisition, Data curation, Conceptualization.

Declaration of competing interest

None.

Data availability

Data will be made available on request.

Acknowledgments

We thank Claudio Rivera for providing anti-cofilin and anti-phosphorylated cofilin antibodies and the Molecular and Cellular Biology Facility (PBMC), the Animal Core Facility and the Imaging Facility (inMagic) INMED platforms, Lucas Silvagnoli and Tangra Draia-Nicolau for their technical support.

This work was supported by the Institut National de la Santé et de la Recherche Médicale, European Community 7th Framework programs (Development and Epilepsy—Strategies for Innovative Research to improve diagnosis, prevention and treatment in children with difficult to treat Epilepsy [DESIRE], Health-F2-602531-2013 (A. F., A. R., C.C.), Fritz Thyssen Stiftung - 10.15.2.022MN (C. C and A.F.), Fondation Jérôme Lejeune - 1159-CC2013A (C.C), the French National Center for Scientific Research (A.R.) and by Ian Excellence Initiative of Aix–Marseille University/A*MIDEX grant (CALIN -R24002AA) of the French 'Investissements d'Avenir' programme. F. C. G. was supported by a postdoctoral fellowship from Fondazione Umberto Veronesi.

Appendix A. Supplementary data

Supplementary data to this article can be found online at https://doi.org/10.1016/j.nbd.2024.106558.

References

Aghakhani, Y., Kinay, D., Gotman, J., Soualmi, L., Andermann, F., Olivier, A., Dubeau, F., 2005. The role of periventricular nodular heterotopia in epileptogenesis. Brain 128, 641–651. https://doi.org/10.1093/brain/awh388.

Aprea, J., Nonaka-Kinoshita, M., Calegari, F., 2014. Generation and characterization of Neurod1-CreER(T2) mouse lines for the study of embryonic and adult neurogenesis. Genesis 52, 870–878. https://doi.org/10.1002/dvg.22797.

Ayala, R., Shu, T., Tsai, L.H., 2007. Trekking across the brain: the journey of neuronal migration. Cell 128, 29–43. https://doi.org/10.1016/j.cell.2006.12.021.

Bamburg, J.T., Minamide, L.S., Wiggan, O., Tahtamouni, L.H., Kuhn, T.B., 2021. Cofilin and actin dynamics: multiple modes of regulation and their impacts in neuronal development and degeneration. Cells 10, 2726. https://doi.org/10.3390/cells10102726.

Banka, S., Bennington, A., Baker, M.J., Rijckmans, E., Clemente, G.D., Ansor, N.M., Sito, H., Prasad, P., Anyane-Yeboa, K., Badalato, L., et al., 2022. Activating RAC1 variants in the switch II region cause a developmental syndrome and alter neuronal morphology. Brain 145, 4232–4245. https://doi.org/10.1093/brain/awac049.

Bär, J., Kobler, O., van Bommel, B., Mikhaylova, M., 2016. Periodic F-actin structures shape the neck of dendritic spines. Sci. Rep. 6, 37136. https://doi.org/10.1038/srep37136.

Bokoch, G.M., 2003. Biology of the p21-activated kinases. Annu. Rev. Biochem. 72, 743–781. https://doi.org/10.1146/annurev.biochem.72.121801.161742.

Bozzi, Y., Provenzano, G., Casarosa, S., 2018. Neurobiological bases of autism-epilepsy comorbidity: a focus on excitation/inhibition imbalance. Eur. J. Neurosci. 47, 534–548. https://doi.org/10.1111/ejn.13595.

Carabalona, A., Beguin, S., Pallesi-Pocachard, E., Buhler, E., Pellegrino, C., Arnaud, K., Hubert, P., Oualha, M., Siffroi, J.P., Khantane, S., et al., 2012. A glial origin for periventricular nodular heterotopia caused by impaired expression of Filamin-a. Hum. Mol. Genet. 21, 1004–1017. https://doi.org/10.1093/hmg/ddr531.

Chai, X., Zhao, S., Fan, L., Zhang, W., Lu, X., Shao, H., Wang, S., Song, L., Failla, A.V., Zobiak, B., Mannherz, H.G., Frotscher, M., 2016. Reelin and cofilin cooperate during the migration of cortical neurons: a quantitative morphological analysis. Development 143, 1029–1040. https://doi.org/10.1242/dev.134163.

Cingolani, L.A., Goda, Y., 2008. Actin in action: the interplay between the actin cytoskeleton and synaptic efficacy. Nat. Rev. Neurosci. 9, 344–356. https://doi.org/10.1038/nrn2373.

Costa, J.F., Dines, M., Lamprecht, R., 2020. The role of Rac GTPase in dendritic spine morphogenesis and memory. Front. Synaptic. Neurosci. 12, 12. https://doi.org/10.3389/fnsyn.2020.00012.

de Curtis, I., 2008. Functions of Rac GTPases during neuronal development. Dev. Neurosci. 30, 47–58. https://doi.org/10.1159/000109851.

Dubeau, F., Tampieri, D., Lee, N., Andermann, E., Carpenter, S., Leblanc, R., Olivier, A., Radtke, R., Villemure, J.G., Andermann, F., 1995. Periventricular and subcortical nodular heterotopia. A study of 33 patients. Brain 118, 1273–1287. https://doi.org/10.1093/brain/118.5.1273.

Edwards, D.C., Sanders, L.C., Bokoch, G.M., Gill, G.N., 1999. Activation of LIM-kinase by Pak1 couples Rac/Cdc42 GTPase signalling to actin cytoskeletal dynamics. Nat. Cell Biol. 11 (5), 253–259. https://doi.org/10.1038/12963.

Falace, A., Buhler, E., Fadda, M., Watrin, F., Lippiello, P., Pallesi-Pocachard, E., Baldelli, P., Benfenati, F., Zara, F., Represa, A., et al., 2014. TBC1D24 regulates neuronal migration and maturation through modulation of the ARF6-dependent pathway. Proc. Natl. Acad. Sci. USA 111, 2337–2342. https://doi.org/10.1073/pnas.1316294111.

Feng, Y., Chen, M.H., Moskowitz, I.P., Mendonza, A.M., Vidali, L., Nakamura, F., Kwiatkowski, D.J., Walsh, C.A., 2006. Filamin a (FLNA) is required for cell-cell contact in vascular development and cardiac morphogenesis. Proc. Natl. Acad. Sci. USA 103, 19836–19841. https://doi.org/10.1073/pnas.0609628104.

Ferland, R.J., Batiz, L.F., Neal, J., Lian, G., Bundock, E., Lu, J., Hsiao, Y.C., Diamond, R., Mei, D., Banham, A.H., et al., 2009. Disruption of neural progenitors along the ventricular and subventricular zones in periventricular heterotopia. Hum. Mol. Genet. 18, 497–516. https://doi.org/10.1093/hmg/ddn377.

Fox, J.W., Lamperti, E.D., Ekşioğlu, Y.Z., Hong, S.E., Feng, Y., Graham, D.A., Scheffer, I. E., Dobyns, W.B., Hirsch, B.A., Radtke, R.A., et al., 1998. Mutations in filamin 1 prevent migration of cerebral cortical neurons in human periventricular heterotopia. Neuron 21, 1315–1325. https://doi.org/10.1016/s0896-6273(00)80651-0.

Fry, A.E., Kerr, M.P., Gibbon, F., Turnpenny, P.D., Hamandi, K., Stoodley, N., Robertson, S.P., Pilz, D.T., 2013. Neuropsychiatric disease in patients with periventricular heterotopia. J. Neuropsychiatr. Clin. Neurosci. 25, 26–31. https://doi.org/10.1176/appi.neuropsych.11110336.

Gardel, M.L., Nakamura, F., Hartwig, J.H., Crocker, J.C., Stossel, T.P., Weitz, D.A., 2006. Prestressed F-actin networks cross-linked by hinged filamins replicate mechanical properties of cells. Proc. Natl. Acad. Sci. USA 103, 1762–1767. https://doi.org/10.1073/pnas.0504777103.

Gilman, S.R., Iossifov, I., Levy, D., Ronemus, M., Wigler, M., Vitkup, D., 2011. Rare *de novo* variants associated with autism implicate a large functional network of genes involved in formation and function of synapses. Neuron 70, 898–907. https://doi.org/10.1016/j.neuron.2011.05.021.

Golden, S.A., Christoffel, D.J., Heshmati, M., Hodes, G.E., Magida, J., Davis, K., Cahill, M. E., Dias, C., Ribeiro, E., Ables, J.L., et al., 2013. Epigenetic regulation of RAC1 induces synaptic remodeling in stress disorders and depression. Nat. Med. 19, 337–344. https://doi.org/10.1038/nm.3090.

Gross, G.G., Junge, J.A., Mora, R.J., Kwon, H.B., Olson, C.A., Takahashi, T.T., Liman, E. R., Ellis-Davies, G.C., McGee, A.W., Sabatini, B.L., et al., 2013. Recombinant probes for visualizing endogenous synaptic proteins in living neurons. Neuron 78, 971–985. https://doi.org/10.1016/j.neuron.2013.04.017.

Guarnieri, F., Falace, A., de Chevigny, A., Cardoso, C., 2018. Disorders of neurogenesis and cortical development. Dialogues Clin. Neurosci. 20, 255–266. https://doi.org/10.31887/DCNS.2018.20.4/ccardoso.

Guerrini, R., Dobyns, W.B., 2014. Malformations of cortical development: clinical features and genetic causes. Lancet Neurol. 13, 710–726. https://doi.org/10.1016/S1474-4422(14)70040-7.

Hart, A.W., Morgan, J.E., Schneider, J., West, K., McKie, L., Bhattacharya, S., Jackson, I. J., Cross, S.H., 2006. Cardiac malformations and midline skeletal defects in mice lacking filamin a. Hum. Mol. Genet. 15, 2457–2467. https://doi.org/10.1093/hmg/ddl168.

Hiromoto, Y., Azuma, Y., Suzuki, Y., Hoshina, M., Uchiyama, Y., Mitsuhashi, S., Miyatake, S., Mizuguchi, T., Takata, A., Miyake, N., et al., 2020. Hemizygous FLNA variant in West syndrome without periventricular nodular heterotopia. Hum. Genome. Var. 7, 43. https://doi.org/10.1038/s41439-020-00131-9.

Hotulainen, P., Hoogenraad, C.C., 2010. Actin in dendritic spines: connecting dynamics to function. J. Cell Biol. 189, 619–629. https://doi.org/10.1083/jcb.201003008.

Jan, Y.N., Jan, L.Y., 2010. Branching out: mechanisms of dendritic arborization. Nat. Rev. Neurosci. 11, 316–328. https://doi.org/10.1038/nrn2836.

Jobin, M.L., Siddig, S., Koszegi, Z., Lanoiselée, Y., Khayenko, V., Sungkaworn, T., Werner, C., Seier, K., Misigaiski, C., Mantovani, G., et al., 2023. Filamin a organizes γ-aminobutyric acid type B receptors at the plasma membrane. Nat. Commun. 14, 34. https://doi.org/10.1038/s41467-022-35708-1.

Kaas, J.H., 2013. The evolution of brains from early mammals to humans. Wiley Interdiscip. Rev. Cogn. Sci. 4, 33–45. https://doi.org/10.1002/wcs.1206.

Kandel, E.R., Squire, L.R., 2000. Neuroscience: breaking down scientific barriers to the study of brain and mind. Science 290, 1113–1120. https://doi.org/10.1126/science.290.5494.1113.

Korobova, F., Svitkina, T., 2010. Molecular architecture of synaptic actin cytoskeleton in hippocampal neurons reveals a mechanism of dendritic spine morphogenesis. Mol. Biol. Cell 21, 165–176. https://doi.org/10.1091/mbc.e09-07-0596.

Lee, J.H., Kreitzer, A.C., Singer, A.C., Schiff, N.D., 2017. Illuminating neural circuits: from molecules to MRI. J. Neurosci. 37, 10817–10825. https://doi.org/10.1523/JNEUROSCI.2569-17.2017.

Lian, G., Lu, J., Hu, J., Zhang, J., Cross, S.H., Ferland, R.J., Sheen, V.L., et al., 2012. Filamin a regulates neural progenitor proliferation and cortical size through Wee1-dependent Cdk1 phosphorylation. J. Neurosci. 32, 7672–7684. https://doi.org/10.1523/JNEUROSCI.0894-12.2012.

Lian, G., Wong, T., Lu, J., Hu, J., Zhang, J., Sheen, V., 2019. Cytoskeletal associated Filamin A and RhoA affect neural progenitor specification during mitosis. Cereb. Cortex 29, 1280–1290. https://doi.org/10.1093/cercor/bhy033.

Llano, O., Smirnov, S., Soni, S., Golubtsov, A., Guillemin, I., Hotulainen, P., Medina, I., Nothwang, H.G., Rivera, C., Ludwig, A., 2015. KCC2 regulates actin dynamics in dendritic spines via interaction with β-PIX. J. Cell Biol. 209, 671–686. https://doi.org/10.1083/jcb.201411008.

Lodato, S., Arlotta, P., 2015. Generating neuronal diversity in the mammalian cerebral cortex. Annu. Rev. Cell Dev. Biol. 31, 699–720. https://doi.org/10.1146/annurev-cellbio-100814-125353.

Ma, B., Shan, X., Yu, J., Zhu, T., Li, R., Lv, H., Cheng, H., Zhang, T., Wang, L., Wei, F., et al., 2022. Social deficits via dysregulated Rac1-dependent excitability control of prefrontal cortical neurons and increased GABA/glutamate ratios. Cell Rep. 41, 111722 https://doi.org/10.1016/j.celrep.2022.111722.

Minegishi, T., Kastian, R.F., Inagaki, N., 2023. Mechanical regulation of synapse formation and plasticity. Semin. Cell Dev. Biol. 140, 82–89. https://doi.org/10.1016/j.semcdb.2022.05.017.

Nakamura, F., 2013. FilGAP and its close relatives: a mediator of rho-Rac antagonism that regulates cell morphology and migration. Biochem. J. 453, 17–25. https://doi.org/10.1042/BJ20130290.

Nakamura, F., Heikkinen, O., Pentikäinen, O.T., Osborn, T.M., Kasza, K.E., Weitz, D.A., Kupiainen, O., Permi, P., Kilpeläinen, I., Ylänne, J., et al., 2009. Molecular basis of filamin A-FilGAP interaction and its impairment in congenital disorders associated with filamin a mutations. PLoS One 4, e4928. https://doi.org/10.1371/journal.pone.0004928.

Nelson, A.D., Bender, K.J., 2021. Dendritic integration dysfunction in neurodevelopmental disorders. Dev. Neurosci. 43, 201–221. https://doi.org/10.1159/000516657.

Nestor, M.W., Hoffman, D.A., 2012. Aberrant dendritic excitability: a common pathophysiology in CNS disorders affecting memory? Mol. Neurobiol. 45, 478–487. https://doi.org/10.1007/s12035-012-8265-x.

Nguyen, L.S., Jolly, L., Shoubridge, C., Chan, W.K., Huang, L., Laumonnier, F., Raynaud, M., Hackett, A., Field, M., Rodriguez, J., et al., 2012. Transcriptome profiling of UPF3B/NMD-deficient lymphoblastoid cells from patients with various forms of intellectual disability. Mol. Psychiatry 17, 1103–1115. https://doi.org/10.1038/mp.2011.163.

Noam, Y., Phan, L., McClelland, S., Manders, E.M., Ehrengruber, M.U., Wadman, W.J., Baram, T.Z., Chen, Y., 2012. Distinct regional and subcellular localization of the actin-binding protein filamin a in the mature rat brain. J. Comp. Neurol. 520, 3013–3034. https://doi.org/10.1002/cne.23106.

Ohta, Y., Hartwig, J.H., Stossel, T.P., 2006. FilGAP, a rho- and ROCK-regulated GAP for Rac binds filamin a to control actin remodelling. Nat. Cell Biol. 8, 803–814. https://doi.org/10.1038/ncb1437.

Parrini, E., Ramazzotti, A., Dobyns, W.B., Mei, D., Moro, F., Veggiotti, P., Marini, C., Brilstra, E.H., Dalla Bernardina, B., Goodwin, L., et al., 2006. Periventricular heterotopia: phenotypic heterogeneity and correlation with Filamin A mutations. Brain 129, 1892, 1906. https://doi.org/10.1093/brain/awl125.

Penzes, P., Cahill, M.E., Jones, K.A., Srivastava, D.P., 2008. Convergent CaMK and RacGEF signals control dendritic structure and function. Trends Cell Biol. 18, 405–413. https://doi.org/10.1016/j.tcb.2008.07.002.

Pizzo, F., Roehri, N., Catenoix, H., Medina, S., McGonigal, A., Giusiano, B., Carron, R., Scavarda, D., Ostrowsky, K., Lepine, A., et al., 2017. Epileptogenic networks in nodular heterotopia: a stereoelectroencephalography study. Epilepsia 58, 2112–2123. https://doi.org/10.1111/epi.13919.

Pyronneau, A., He, Q., Hwang, J.Y., Porch, M., Contractor, A., Zukin, R.S., 2017. Aberrant Rac1-cofilin signaling mediates defects in dendritic spines, synaptic function, and sensory perception in fragile X syndrome. Sci. Signal. 10, eaan0852 https://doi.org/10.1126/scisignal.aan0852.

Rakic, P., 2009. Evolution of the neocortex: a perspective from developmental biology. Nat. Rev. Neurosci. 10, 724–735. https://doi.org/10.1038/nrn2719.

Reijnders, M.R.F., Ansor, N.M., Kousi, M., Yue, W.W., Tan, P.L., Clarkson, K., Clayton-Smith, J., Corning, K., Jones, J.R., Lam, W.W.K., et al., 2017. RAC1 missense mutations in developmental disorders with diverse phenotypes. Am. J. Hum. Genet. 10, 466–477. https://doi.org/10.1016/j.ajhg.2017.08.007.

Rodriguez, A., Ehlenberger, D.B., Dickstein, D.L., Hof, P.R., Wearne, S.L., 2008. Automated three-dimensional detection and shape classification of dendritic spines from fluorescence microscopy images. PLoS One 3, e1997. https://doi.org/10.1371/journal.pone.0001997.

Rust, M.B., 2015. ADF/cofilin: a crucial regulator of synapse physiology and behavior. Cell. Mol. Life Sci. 72, 3521–3529. https://doi.org/10.1007/s00018-015-1941-z.

Segura, I., Lange, C., Knevels, E., Moskalyuk, A., Pulizzi, R., Eelen, G., Chaze, T., Tudor, C., Boulegue, C., Holt, M., et al., 2016. The oxygen sensor PHD2 controls dendritic spines and synapses via modification of Filamin a. Cell Rep. 14, 2653–2667. https://doi.org/10.1016/j.celrep.2016.02.047.

Sheen, V.L., 2014. Filamin a mediated Big2 dependent endocytosis: from apical abscission to periventricular heterotopia. Tissue Barr. 2, e29431 https://doi.org/10.4161/tisb.29431.

Sheen, V.L., Feng, Y., Graham, D., Takafuta, T., Shapiro, S.S., Walsh, C.A., 2002. Filamin A and Filamin B are co-expressed within neurons during periods of neuronal migration and can physically interact. Hum. Mol. Genet. 11, 2845–2854. https://doi.org/10.1093/hmg/11.23.2845.

Solé, G., Coupry, I., Rooryck, C., Guérineau, E., Martins, F., Devés, S., Hubert, C., Souakri, N., Boute, O., Marchal, C., et al., 2009. Bilateral periventricular nodular heterotopia in France: frequency of mutations in FLNA, phenotypic heterogeneity and spectrum of mutations. J. Neurol. Neurosurg. Psychiatry 80, 1394–1398. https://doi.org/10.1136/jnnp.2008.162263.

Staley, K., 2015. Molecular mechanisms of epilepsy. Nat. Neurosci. 18, 367–372. https://doi.org/10.1038/nn.3947.

Sutherland-Smith, A.J., 2011. Filamin structure, function and mechanics: are altered filamin-mediated force responses associated with human disease? Biophys. Rev. 3, 15–23. https://doi.org/10.1007/s12551-011-0042-y.

Tahirovic, S., Hellal, F., Neukirchen, D., Hindges, R., Garvalov, B.K., Flynn, K.C., Stradal, T.E., Chrostek-Grashoff, A., Brakebusch, C., Bradke, F., 2010. Rac1 regulates neuronal polarization through the WAVE complex. J. Neurosci. 30, 6930–6943. https://doi.org/10.1523/JNEUROSCI.5395-09.2010.

Threadgill, R., Bobb, K., Ghosh, A., 1997. Regulation of dendritic growth and remodeling by rho, Rac, and Cdc42. Neuron 19, 625–634. https://doi.org/10.1016/s0896-6273(00)80376-1.

Wegiel, J., Kuchna, I., Nowicki, K., Imaki, H., Wegiel, J., Marchi, E., Ma, S.Y., Chauhan, A., Chauhan, V., Bobrowicz, T.W., et al., 2010. The neuropathology of autism: defects of neurogenesis and neuronal migration, and dysplastic changes. Acta Neuropathol. 119, 755–770. https://doi.org/10.1007/s00401-010-0655-4.

Wei, C.M., Xia, G.Z., Ren, R.N., 2018. Gene mutations in unexplained infantile epileptic encephalopathy: an analysis of 47 cases. Zhongguo Dang. Dai. Er. Ke. Za. Zhi. Chin. 20, 125–129. https://doi.org/10.7499/j.issn.1008-8830.2018.02.009.

Xiang, X., Li, S., Zhuang, X., Shi, L., 2016. Arhgef1 negatively regulates neurite outgrowth through activation of RhoA signaling pathways. FEBS Lett. 590, 2940–2955. https://doi.org/10.1002/1873-3468.12339.

Yang, N., Higuchi, O., Ohashi, K., Nagata, K., Wada, A., Kangawa, K., Nishida, E., Mizuno, K., 1998. Cofilin phosphorylation by LIM-kinase 1 and its role in Rac-mediated actin reorganization. Nature 25 (393), 809–812. https://doi.org/10.1038/31735.

Zamboni, V., Armentano, M., Berto, G., Ciraolo, E., Ghigo, A., Garzotto, D., Umbach, A., Di Cunto, F., Parmigiani, E., Boido, M., et al., 2018. Hyperactivity of Rac1-GTPase pathway impairs neuritogenesis of cortical neurons by altering actin dynamics. Sci. Rep. 8, 7254. https://doi.org/10.1038/s41598-018-25354-3.

Zhang, L., Bartley, C.M., Gong, X., Hsieh, L.S., Lin, T.V., Feliciano, D.M., Bordey, A., 2014. MEK-ERK1/2-dependent FLNA overexpression promotes abnormal dendritic patterning in tuberous sclerosis independent of mTOR. Neuron 84, 78–91. https://doi.org/10.1016/j.neuron.2014.09.009.

Zhang, L., Huang, T., Teaw, S., Nguyen, L.H., Hsieh, L.S., Gong, X., Burns, L.H., Bordey, A., 2020. FilaminA inhibition reduces seizure activity in a mouse model of focal cortical malformations. Sci. Transl. Med. 12, eaay0289 https://doi.org/10.1126/scitranslmed.aay0289.